

Thermal Deformation and RF Performance Analyses for the SWOT Large Deployable Ka-Band Reflectarray

H. Fang¹, E. Sunada², J. Chaubell³, D. Esteban-Fernandez⁴, M. Thomson⁵ and F. Nicaise⁶
Jet Propulsion Laboratory, California Institute of Technology, Pasadena, California, 91109-8099

A large deployable antenna technology for the NASA Surface Water and Ocean Topography (SWOT) Mission is currently being developed by JPL in response to NRC Earth Science Tier 2 Decadal Survey recommendations. This technology is required to enable the SWOT mission due to the fact that no currently available antenna is capable of meeting SWOT's demanding Ka-Band remote sensing requirements. One of the key aspects of this antenna development is to minimize the effect of the on-orbit thermal distortion to the antenna RF performance. An analysis process which includes: 1) the on-orbit thermal analysis to obtain the temperature distribution; 2) structural deformation analysis to get the geometry of the antenna surface; and 3) the RF performance with the given deformed antenna surface has been developed to accommodate the development of this antenna technology. The detailed analysis process and some analysis results will be presented and discussed by this paper.

I. Introduction

USA and French oceanographers and hydrologists have joined forces to study a new space mission to make a comprehensive global survey of Earth's surface water, observe the fine details of the ocean's surface topography, and measure how water bodies change over time. The new mission is called Surface Water Ocean Topography, or SWOT. SWOT is one of the four (Tier 2) missions identified by the National Research Council decadal review for implementation by NASA [1].

Figure 1 shows the mission architecture [2, 3] of the SWOT instrument. SWOT will take advantage of interferometric SAR technology, which will allow it to characterize the ocean sub-mesoscale processes down to 10 km scales, thereby enabling for the first time a much higher resolution than the 200-300 km mesoscale processes resolved by today's satellite altimeters. For terrestrial hydrology, current observations are limited to on-site gauges that provide sparse measurements of the Earth's surface water data, such as rivers and lakes, and are unavailable for many regions. SWOT will provide the first global inventory of surface water extent and changes in storage for rivers whose width exceeds 100 m and lakes whose area exceeds 250 m².

¹ Mechanical Engineer, MS 299-100, Senior Member AIAA

² Member of Engineering Staff, MS 125-123, Member AIAA

³ Signal Analysis Engineer, MS 300-235

⁴ Radar system Engineer, MS 321-400

⁵ Principal Engineer, MS 299-100, Senior Member AIAA

⁶ Mechanical System Engineer, MS 321-520, Member AIAA

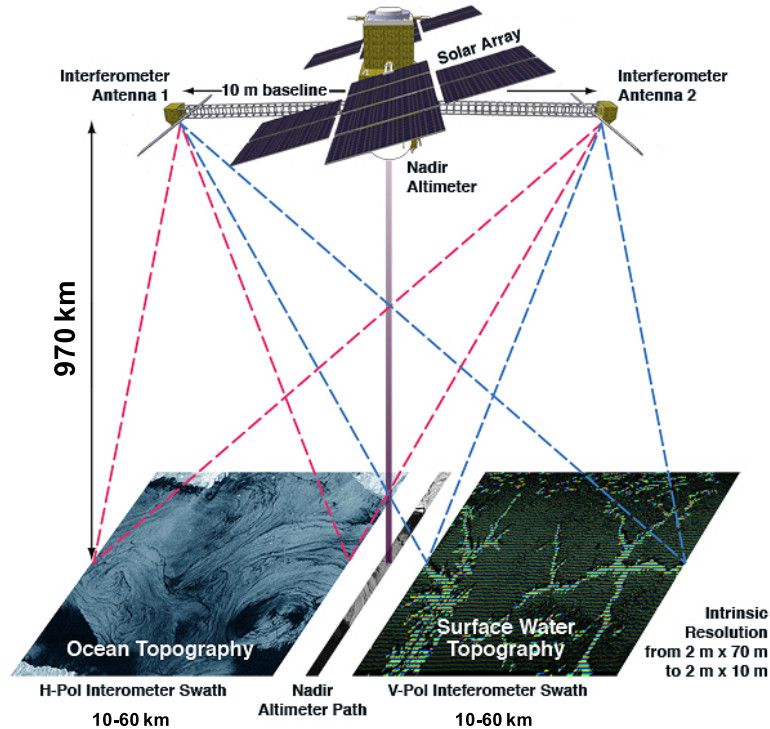


Figure 1. SWOT mission architecture

A radar interferometer concept operating at Ka-band (35.75 GHz) enables this kind of high-resolution extent and elevation measurements. The satellite will fly two radar reflectarray antennas at both ends of a 10-m mast, allowing it to image the elevation of the surface within a 140-kilometer swath centered on the satellite's nadir track. This radar system, termed KaRIn (Ka-band Radar Interferometer), is conceptually similar to NASA's Shuttle Radar Topography Mission, which made high-resolution measurements of Earth's land surface in 2000.

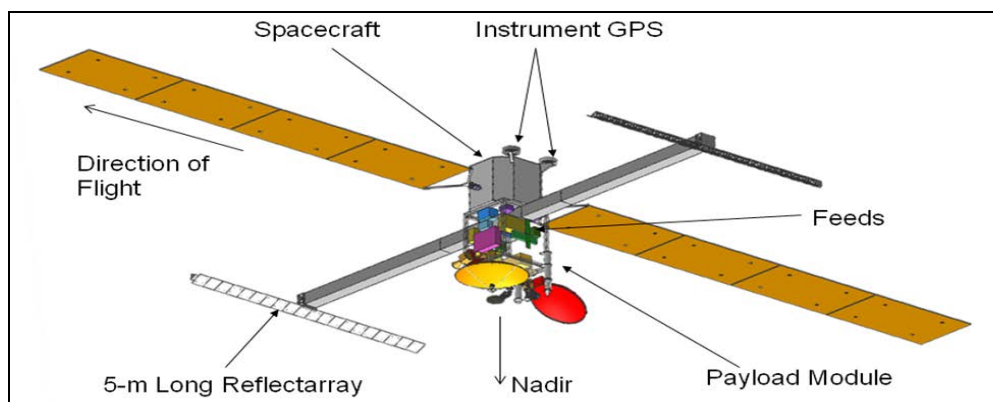


Figure 2. Major components of the Ka-Band radar system

Figure 2 shows the major components of the Ka-Band radar system. The mission concept uses two reflectarray antennas to measure the ocean surface altitude. The two antennas are deployed laterally to obtain a final separation distance of 10 meters, centered on the spacecraft centerline by means of a deployable mast. The radar electronics and antenna feeds are all mounted on the

payload module. Two reflectarray antennas are connected by a mast and the functions of this deployable mast include: (1) support the two reflectarray antennas and stow within the available volume inside the fairing; (2) deploy the two reflectarray antennas and lock into position; (3) have sufficient stiffness to meet the structural frequency requirements; and (4) maintain the two reflectarrays orientations while orbiting.

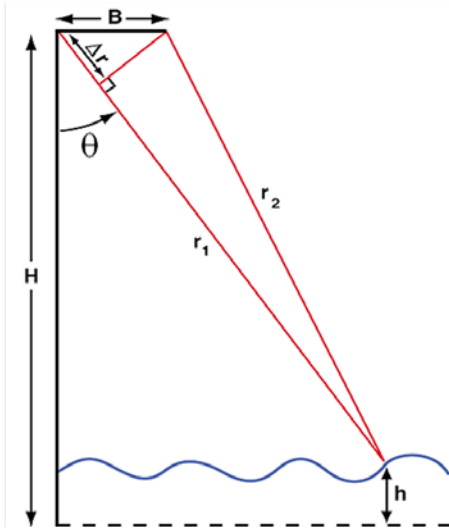


Figure 3. Illustration of the interferometry process

As illustrated in figure 3, interferometry is basically triangulation. The difference between the two sides, Δr , is obtained from the phase difference (Φ) between the two radar channels. The elevation, h , is obtained by equations 1 and 2.

$$\Phi = 2 \frac{2\pi}{\lambda} \Delta r = \frac{2\pi}{\lambda} B \sin(\theta) \quad (1)$$

$$h = H - r \cos(\theta) \quad (2)$$

The mechanical stability of the baseline B (separation between two reflectarrays), as well as the reflectarray pointing accuracy is essential for the success of the SWOT mission. Due to the fact that no currently available antenna is capable of meeting SWOT's challenging structural stability and precision requirements, an antenna system technology is being developed at JPL for the SWOT mission. To accommodate this development, an in-space thermal distortion analysis process has been developed to evaluate antenna RF performances of different antenna designs. This process includes the on-orbit thermal analysis to obtain the temperature distribution; structural deformation analysis to get the deformation of the antenna surface; and the RF performance with the given antenna surface distortions. Figure 4 illustrates the analysis procedure. Details of these steps are discussed in the following sections.

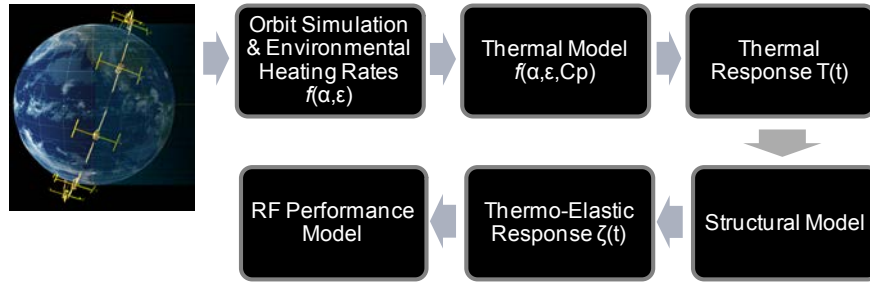


Figure 4. Analysis procedure

II. Thermal model and temperature distribution analysis

Thermal Disturbances

A major disturbance to on-orbit performance stems from environmental heating transients. SWOT is to fly in low Earth orbit at an approximate altitude of 970 km and 78° inclination. The angle between the solar vector and orbit plane (beta angle) can range anywhere between $-90^\circ < \beta < +90^\circ$. Because SWOT must fly with its KaRIN arrays in a specific nadir orientation, the change in environmental heating rates can be significant. Shadowing of portions of the instrument by other spacecraft surfaces and periods during eclipse entry/exit can result in sudden changes in incident solar flux. Earth IR and Earth albedo loads are less of disturbance drivers due to their diffuse nature and the relative constant orientation of the SWOT KaRIN payload to Earth. Figure 5 shows a typical solar flux contour plot at a given instant in time. The effect of shadowing by other spacecraft surfaces can be seen. Figure 6 shows the incident solar flux over a given orbit for two adjacent truss members.

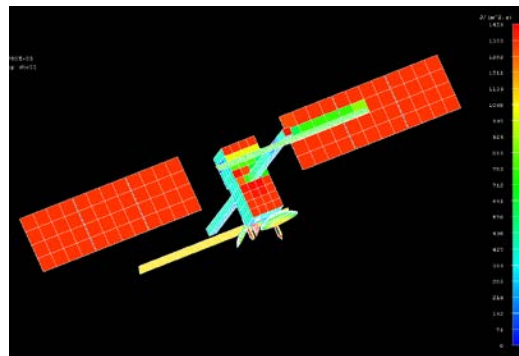


Figure 5a. False-color map indicating the magnitude of incident solar flux on SWOT surfaces. The figure view is that from the Sun direction.

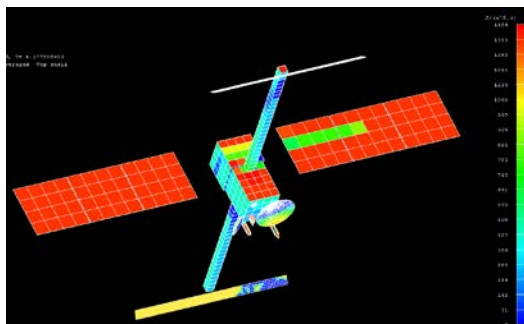


Figure 5b. View rotated to show the absence of incident solar flux on those surfaces in shadow of others.

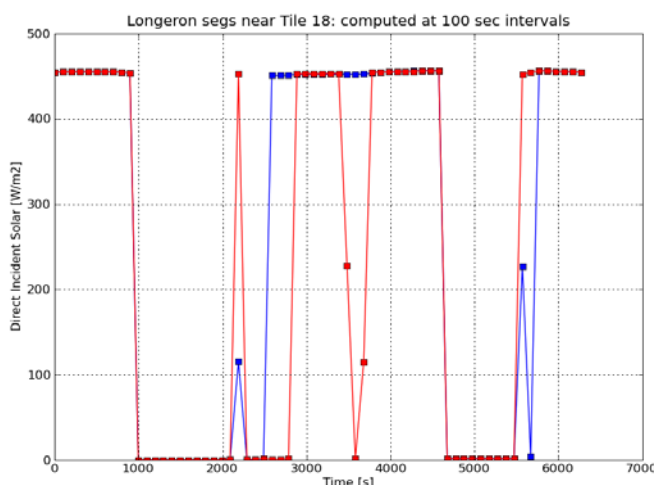


Figure 6. Incident solar insolation on two adjacent truss members for a beta 70° orbit scenario. Changes in flux are significant, as well as differences in flux between adjacent structure.

Thermal Design Description

The KaRIN payload thermal design is predominantly a passive one. Multi-layer insulation (MLI) blankets are used, where possible, to minimize the effect of changing environmental fluxes. Low solar absorptivity coatings are used in other areas to minimize the effect of solar flux transients. The only active thermal control elements are the thermostatically controlled survival heaters used on deployment mechanisms.

The Mast assembly is covered with 17-layer MLI. The outer surface is second-surface aluminized Kapton where the external layer has a solar absorptivity/IR emissivity ratio of 0.41/0.72 end-of-life. The MLI significantly dampens the effects of environmental disturbances.

The nadir-facing surfaces of the KaRIN array panels are not coated with any thermal control materials due to performance restrictions. The zenith side is blanketed with 17-layer MLI. The truss longerons, battens, and diagonals are coated with 0.5-mil aluminized Kapton. The aluminum fittings are coated with 10-mil silverized Teflon tape. Blankets are not used on the truss assembly because of risks to deployments and to minimize system mass.

Thermal Model Description

The thermal model was built and exercised in the IDEAS/TMG thermal tool. About 7500 elements were used, and more than half were dedicated to the KaRIN array and truss assembly. Figure 7 gives a view of the mesh size used.

Geometric view factors and orbital heating rates were generated for several orbit scenarios. The number of positions for which orbital heating rates were calculated over a given orbit was also varied to compare sensitivity to performance. Once completed, the thermal math model was exercised over the required number of orbits to reach pseudo-steady-state conditions. A series of comparison runs were performed for different compute step intervals. Intervals ranged from 10 seconds to 0.05 seconds. The purpose of the smaller time steps was largely for confirmation that thermal induced deformations are not of higher frequencies and also as a test of numerical stability.

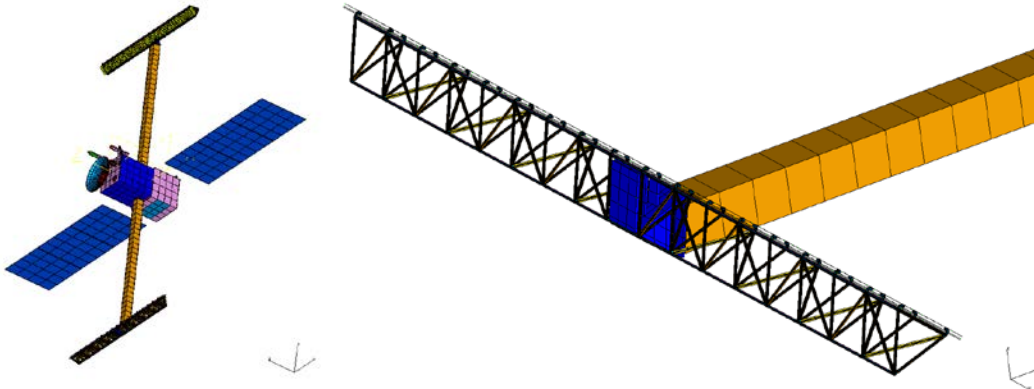


Figure 7. The KaRIN panels were modeled using plate elements to represent facesheets and honeycomb core. The truss members were modeled using beam elements.

Temperature Predictions

Temperature predictions for a matrix of simulations were generated. The run matrix captures the studies done for sensitivity on system performance and consisted of various thermal control coatings, computational time intervals, and orbit scenarios. The transient temperature predictions were then mapped to the structural finite element model (FEM) for the thermo-elastic structural deformation analysis.

III. Structural model and deformation analysis

Due to this study focuses on the two reflectarrays' thermal deformation analyses, only those components that contribute to the reflectarrays thermal deformation are included in the structural Finite Element Model. Major components include a 10-m long mast; two 5-m long trusses which are located at two ends of the mast; 18 reflectarray panes that are supported by two trusses; and

two center bodies that connect the two trusses to the mast. Figure 8 shows one half of the structural model.

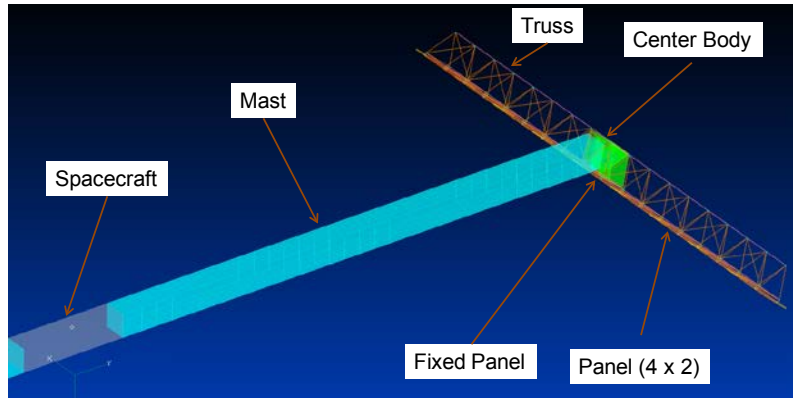


Figure 8. Major components of the structural FEM

Ninety solid elements with total mass of 1000 Kg are placed in the middle of the mast to simulate the mass of the spacecraft. The Coefficient of Thermal Expansion (CTE) of these 90 elements is set to be zero to exclude the spacecraft thermal deformation. The mast is made of 2.25-mm thick low CTE composite material and is modeled by 1530 laminate elements.

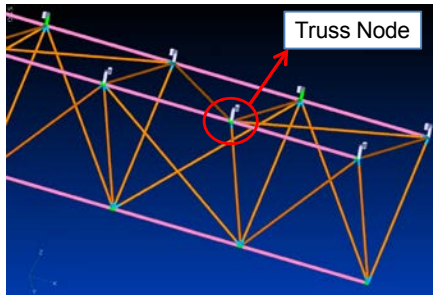


Figure 9. Finite Element the model of the truss

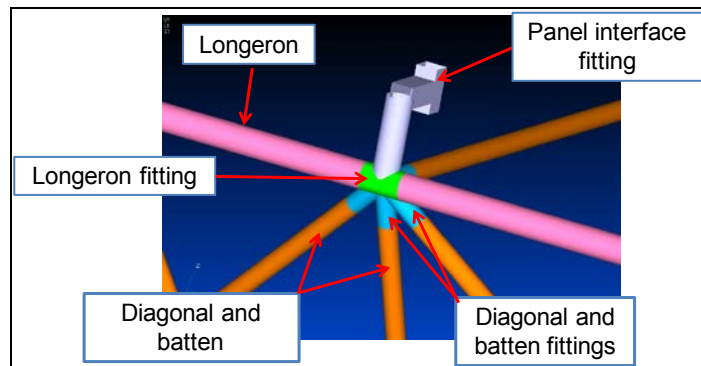


Figure 10. Truss node

Figure 9 shows the model of the truss and Figure 10 is the close-up view of the truss node. The diameter of the longeron is 7.95 mm. The diagonal and batten have the same diameter and the diameter is 5.54 mm. Longerons, diagonals and battens are made of low CTE composite

rods. The panel interface fittings provide the connections between the trusses and the panels. All fittings are made of aluminum. Every truss is modeled by 1215 bar elements.

The reflectarray panels are sandwich panels. The core of a panel is 12.7-mm thick aluminum honeycomb and is modeled by solid elements. The material for the facesheet is 0.3 mm thick Rogers material. Facesheets are modeled by plate elements. Eighteen panels are modeled by 1152 plate elements and 576 solid elements. In order to eliminate the panel bowing introduced by the in-plane displacement mismatch between the trusses and the panels, mechanisms have been designed to release the degrees of freedom between the panel and the truss. Figure 11 illustrates the boundary conditions of a panel. All rotational degrees of freedom at four connecting points are released. The y direction translation at point 2 and x direction translation at point 3 is released. Both x and y translations at point 4 are also released.

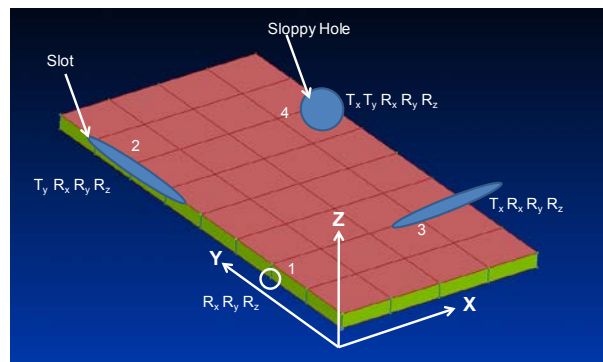


Figure 11. Released degrees of freedom at four connecting points of a panel

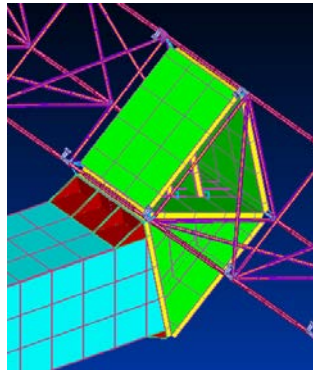


Figure 12. FEM of the center body

The center body connects the truss to the mast as illustrated in Figure 12. It is made of sandwich panels with 12.7-mm thick aluminum honeycombs and 0.75 mm thick composite laminate facesheets.

After the structural FEM is completed, the temperature distribution at every time step is mapped from thermal FEM to structural FEM. Figure 13 illustrates the temperature distribution at one time step. The original temperature is set to room temperature (20 C°) and the temperature deviation from 20 C° introduces structural deformation due to material thermal expansion. After the temperature gradients, namely thermal loads, are mapped onto the structural FEM, structural

deformations are then calculated and Figure 14 shows the structural deviation at one time step. These deviation data are then used to geometrically analyze the RF performances.

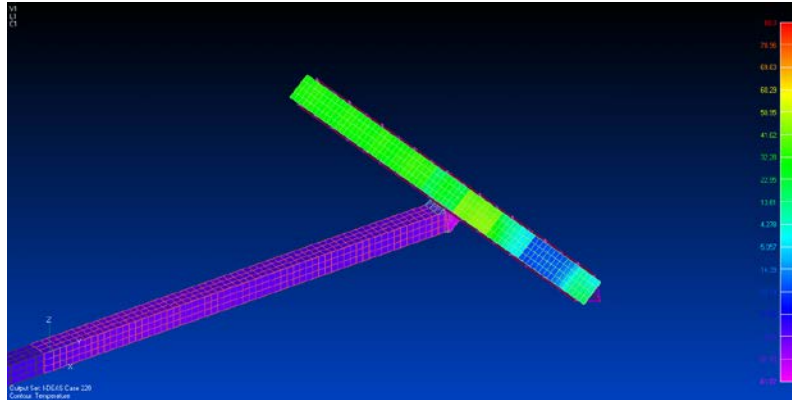


Figure 3. Temperature distribution at one time step

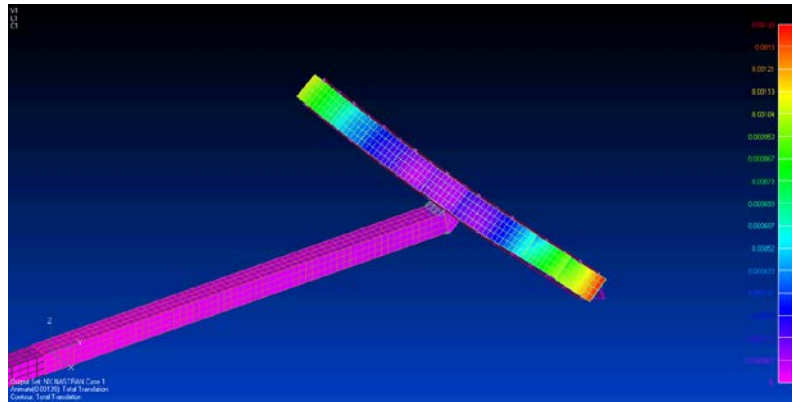


Figure 14. Structural deviation at one time step

IV. RF performance analyses and examples

RF performance is evaluated by elevation (cross-track) pointing error, azimuth (along track) pointing error, baseline dilation error and roll drift error. Definitions of these performance errors and some analysis results are discussed in this section.

1. Elevation pointing error and azimuth pointing error

Elevation pointing is associated to any mechanical distortions (rotations and/or bending) that cause the beams to wander in the YZ plane, while azimuth pointing is associated to the beams wandering in the XY plane. This is illustrated in the Figure 15, where a Cartesian coordinate system is defined at each end of the mast, with the flight direction along the X axis. The pointing direction of the beams is represented by the normal vectors to each antenna plane, n_1 and n_2 . At a given point in time, n_1 and n_2 are the instantaneous pointing vectors accounting for any distortion (rotation, torsion and/or bending).

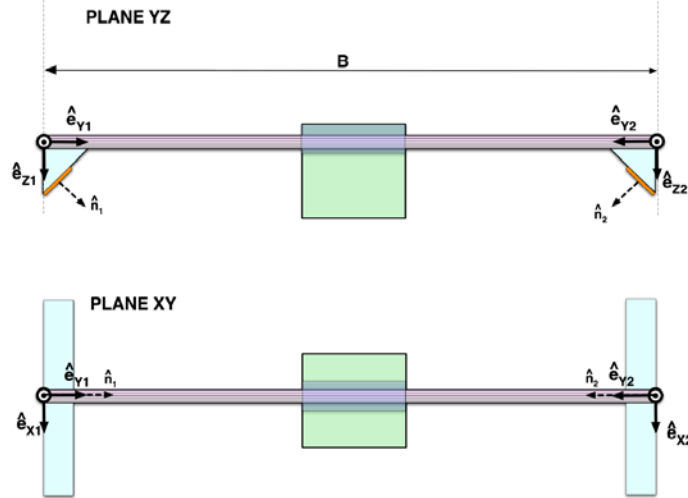


Figure 15. Reference systems used to define the pointing requirements. The payload module is shown in green.

The elevation pointing associated to the fact that both beams must overlap on the ground, which can be expressed as the maximum angle $\Delta\theta$ between n_1 (and n_2) and the XZ plane:

$$\sin^{-1}\left(\frac{|\mathbf{e}_y \cdot \mathbf{n}_{i=1,2}|}{|\mathbf{e}_y| |\mathbf{n}_{i=1,2}|}\right) \leq \Delta\theta \quad (3)$$

The azimuth pointing has multiple components:

- First, there is a relative control component to ensure that the two antenna beams overlap in this direction. Since this is a relative pointing component between both beams, it excludes common modes. This relative mis-pointing can e.g. arise from an anti-symmetric rotation of the mast at both ends, as well as from a bend of the mast in the XY plane. This relative pointing error can thus be expressed using the antenna pointing vectors as $n_1 - n_2 \leq \delta_n$, where δ_n is the maximum mis-pointing vector, and this requirement dictates the maximum angle $\delta\phi$ between the vector δ_n and the YZ plane:

$$\sin^{-1}\left(\frac{|\mathbf{e}_x \cdot \delta_n|}{|\mathbf{e}_x| |\delta_n|}\right) \leq \delta\phi \quad (4)$$

- Second, there is an absolute control component to ensure that both beams are pointed toward nadir. This is a common (symmetric) rotation requirement, which can be expressed as the maximum angle $\delta\phi$ between n_1 (and n_2) and the YZ plane as follows:

$$\sin^{-1}\left(\frac{|\mathbf{e}_x \cdot \mathbf{n}_{i=1,2}|}{|\mathbf{e}_x| |\mathbf{n}_{i=1,2}|}\right) \leq \Delta\phi, \quad (5)$$

2. Baseline dilation error and roll drift error

As with any interferometer, a change in the baseline length and its orientation directly impacts the precision of the height measurements that can be obtained. For SWOT, the baseline length is to be understood as the projection onto the YZ plane of the line that crosses the two reference coordinate systems previously defined at each end of the mast, and the baseline roll as the angle between that projected line and the Y axis (see Figure 16).

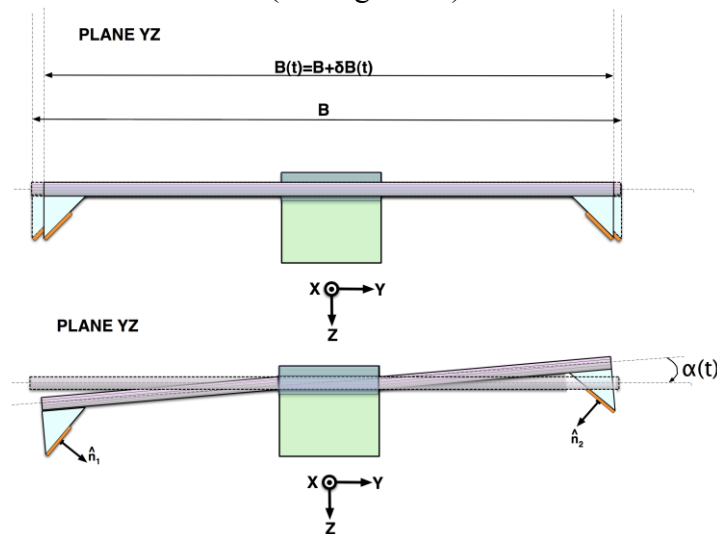


Figure 16. The baseline dilation (top) and baseline roll (bottom) drifts.

Therefore, any thermal contraction or expansion (dilation) of the mast will result in a change of the baseline length formed by the deployed mast. On the other hand, if the mast bends in a non-symmetrical fashion, the baseline will depart from being a line parallel to the Y axis, thereby effectively introducing a baseline roll.

3. Examples of performance analysis results

In order to investigate the feasibility of this mission architecture with currently available low CTE composite materials, several designs have been developed and analyzed. This section presents some performance analysis results of one design. Figure 17 shows elevation pointing errors for different beta angles; Figure 18 shows relative azimuth pointing errors for different beta angles; Figure 19 shows absolute azimuth pointing errors for different beta angles; Figure 20 shows baseline rolls for different beta angles; and Figure 21 shows baseline dilations for different beta angles.

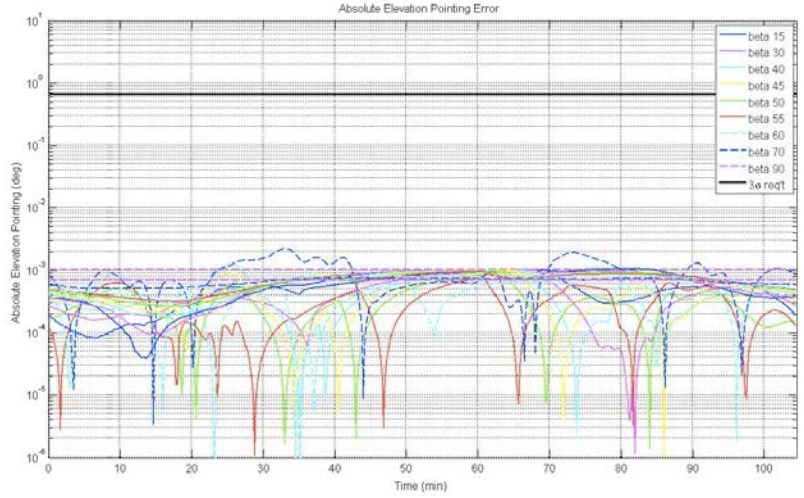


Figure 17. Elevation pointing errors for different beta angles

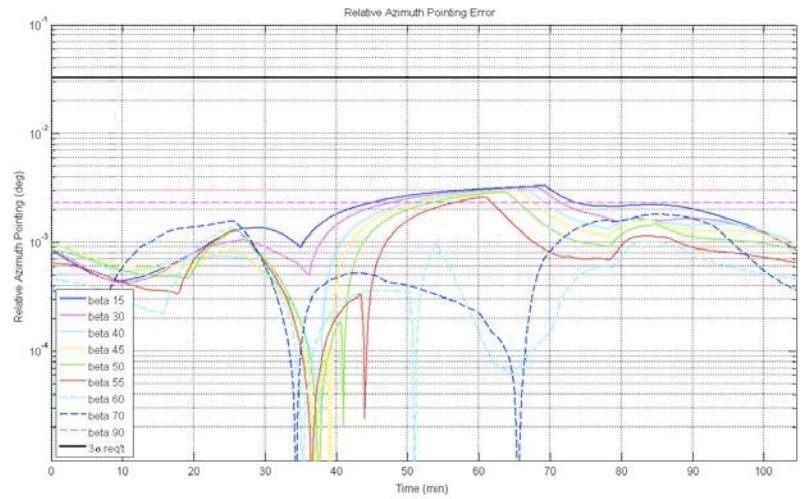


Figure 18. Relative azimuth pointing errors for different beta angles

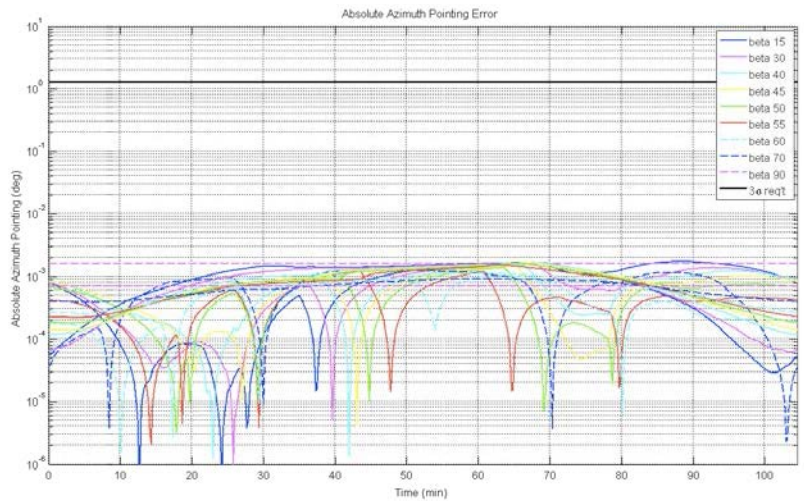


Figure 19. Absolute azimuth pointing errors for different beta angles

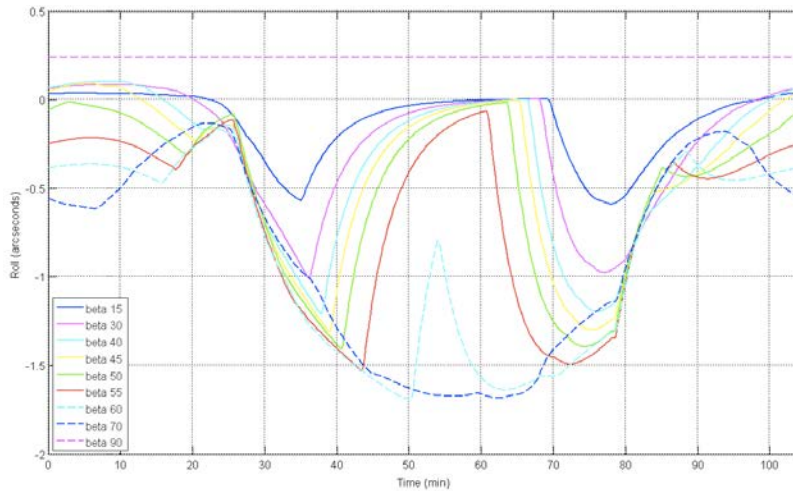


Figure 20. Baseline rolls for different beta angles

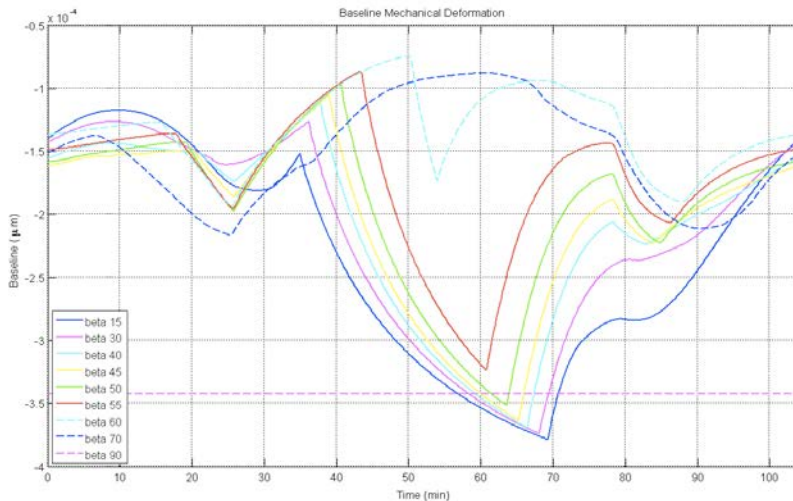


Figure 21. Baseline dilations for different beta angles

V. Conclusions

A performance analysis process has been established to support the development of the antenna system technology for the SWOT mission. Several antenna systems have been designed and the geometrical RF performances of all these systems have been analyzed and evaluated. It is demonstrated by this study that the SWOT mission concept is feasible with currently available low CTE composite materials. With the help of this analysis process, the best design has been identified and an engineering model is being fabricated to further advance this antenna system technology.

Acknowledgments

The work described was performed at Jet Propulsion Laboratory, California Institute of Technology under a contract with the National Aeronautics and Space Administration.

References

¹Laurence C. Smith and Tamlin M. Pavelsky, "Remote sensing of volumetric storage changes in lakes." *EARTH SURFACE PROCESSES AND LANDFORMS* Earth Surf. Process. Landforms 34, 1353–1358 (2009), John Wiley & Sons, Ltd., 2 June 2009, Wiley InterScience, DOI: 10.1002/esp.1822.

²Fu, L-L, D. Alsdorf, E. Rodriguez, R. Morrow, N. Mognard, J. Lambin, P. Vaze, and T. Lafon, "The SWOT (Surface Water and Ocean Topography) Mission: Spaceborne Radar Interferometry for Oceanographic and Hydrological Applications." *OCEANOBS'09 Conference*, 2009.

³<http://nasascience.nasa.gov/earth-science/decadal-surveys>